Research paper

Note on the compatibility of ICOS, NEON, and TERN sampling designs, different camera setups for effective plant area index estimation with digital hemispherical photography

Mihkel Kaha[1], Mait Lang[1,2*], Shaohui Zhang[3] and Jan Pisek[1]

Kaha, M., Lang, M., Zhang, S., Pisek, J. 2023. Note on the compatibility of ICOS, NEON, and TERN sampling designs, different camera setups for effective plant area index estimation with digital hemispherical photography. – Forestry Studies | Metsanduslikud Uurimused 79, 21–36, ISSN 1406-9954. Journal homepage: http://mi.emu.ee/forestry.studies

Abstract. Environmental monitoring networks such as the Integrated Carbon Observation System (ICOS) in Europe, the National Ecological Observatory Network (NEON) in the U.S., or the Terrestrial Ecosystem Research Network (TERN) in Australia deploy different sampling schemes for in situ measurements. We report on the intercomparison of measurements of the canopy gap fraction with different digital hemispherical photography setups adopting ICOS, NEON, and TERN sampling schemes. The test was carried out at the Järvselja Radiation Transfer Model Intercomparison (RAMI) birch stand. Results show that spreading out sampling points which cover more of the plot is important for a good representation of the forest as a whole. The NEON tower plot layout scheme may be more prone to errors in overall canopy properties estimation than ICOS or TERN due to its compact sampling layout and should always be used in conjunction with its distributed plots. Different camera setups involving different camera operators, camera bodies, lenses and settings yield slightly varied results, and it is important to ensure that the images are taken in such a way that they would not be over or underexposed, or out of focus. As a conclusion we recommend always to carry out intercomparison measurements with old and new cameras when devices are upgraded. Our study contributes towards establishing the uncertainty and evaluating potential error budget stemming from collecting in situ measurements using different sampling schemes and camera setups.

Key words: ICOS, NEON, TERN, digital hemispherical photography, plant area index, RAMI.

Authors' addresses: [1]Tartu Observatory, University of Tartu, 61602 Tõravere, Estonia; [2]Institute of Forestry and Engineering, Estonian University of Life Sciences, Kreutzwaldi 5, 51006 Tartu, Estonia; [3]School of Forest Sciences, University of Eastern Finland, Yliopistokatu 7, FI-80101 Joensuu, Finland; *e-mail: mait.lang@emu.ee

Introduction

Leaf Area Index (LAI), a measure of the amount of plant leaf material in an ecosystem, is defined as one half of the total green leaf area per unit ground surface area (Chen & Black, 1992; Fernandes *et al.*, 2014). LAI is included in many models describing vegetation-atmosphere interactions (GCOS-138, 2010) as a critical variable controlling processes such as photosynthesis, respiration, and rain interception. LAI

DOI: 10.2478/fsmu-2023-0010

estimates using different Earth Observation (EO) data and algorithms have been developed and made available to the user community over the last decades (Fang *et al.*, 2019) as ready-for-use products. When no adjustments are made for the clumping effect or for the interception of light by woody canopy elements when estimating LAI, the variable is the effective Plant Area Index (PAI_e) instead (Chen, 1996).

The Global Climate Observing System (GCOS) has specified the need to update and validate global LAI predictions systematically. The Land Product Validation (LPV) sub-group of the Committee for Earth Observation Satellites (CEOS) developed a strategy for validating the predictions (Fernandes *et al.*, 2014). The CEOS LPV currently encourages validation and intercomparison of the so-called LPV Supersites. The majority of the LPV Supersites come from well-known and established networks, including the Integrated Carbon Observation System (ICOS) (Gielen *et al.*, 2017) in Europe, the National Ecological Observatory Network (NEON) (Meier & Jones, 2018) in the U.S., and the Terrestrial Ecosystem Research Network (TERN) (Karan, 2015) in Australia. However, the networks employ different sampling designs (i.e. number of measurements, location of sampling points within the test site) and camera setups for in situ LAI estimation. Previous studies have reported apparent differences in the LAI estimates from different sampling schemes (Calders *et al.*, 2018; Liu *et al.*, 2021; Majasalmi *et al.*, 2012; Nackaerts *et al.*, 2000; Zou *et al.*, 2020).

The objective of this study is to compare the three different schemes adopted within the ICOS, NEON, and TERN networks instead of searching for the most optimal, new sampling scheme. We carried out the intercomparison measurements with digital hemispherical photography during diffuse light conditions, adopting the established ICOS, NEON, and TERN sampling schemes. We use data from a measurement campaign conducted in 2021 at the Järvselja Radiation Transfer Model Intercomparison (RAMI) (Widlowski *et al.*, 2015) birch stand. The impacts of the sampling schemes and camera setups on the gap fraction and (PAI_e) prediction and estimation from digital hemispherical photography (DHP) were analysed.

Material and Methods

Study site

The measurements were conducted in a 63-year-old, mature fertile silver birch (*Betula pendula* Roth) forest stand in Järvselja, Estonia (58°16′ 49.81″ N, 27°19′ 51.53″ E), which belongs to the RAMI dataset (Widlowski *et al.*, 2015). It is an intensively studied site that serves in various forest reflectance modelling and remote sensing experiments. The dominating upper layer has a basal area of 28.2 m^2 ha^{-1} that is distributed between silver birch 55%, common alder (*Alnus glutinosa* (L.) Gaertn.) 31%, and European aspen (*Populus tremula* L.) 14%. The stocking density was 966 trees per hectare according to 2019 measurements (Lang *et al.*, 2021). Kuusk *et al.* (2013, 2009) and Lang *et al.* (2021) have given a more detailed site description. The stand contains a 100 m × 100 m sample plot, within which all digital hemispherical photographs were taken (Figure 1). Lang & Pisek (2019) describe the changes in the canopy gap fraction regarding the growth of the forest stand understorey and dominant tree layer.

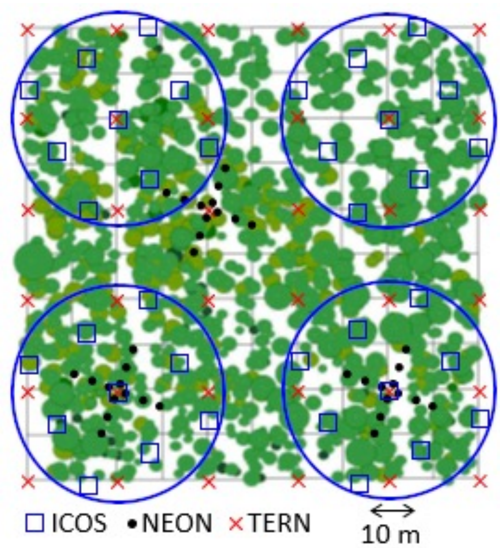

Figure 1. Positions for digital hemispherical photography within the test site of Järvselja RAMI birch stand.

Joonis 1. Mõõtmispunktide asukohad Järvseljal RAMI kaasikus vastavalt erinevatele skeemidele.

Data acquisition and processing

Three sampling schemes corresponding to the ICOS, NEON, and TERN schemes (each consisting of 36 individual sampling points) were used in this study (Figure 1). The ICOS (Gielen *et al.*, 2017) scheme has four circular continuous plots, each consisting of 9 sampling points. The NEON (Meier & Jones, 2018) scheme has three "tower" type plots that consist of 12 sampling points in a cross pattern oriented in the cardinal directions. The TERN (Karan, 2015) scheme is a regular 6 by 6 grid of measurement points across the whole plot. The position of each sampling point in the field was established with a land survey tape and a compass, and marked with stakes and flags to facilitate the DHP image collection.

Three camera setups were used (Table 1), with each operated by a different individual. At each sampling point, the DHP images were taken in immediate sequence with the three different camera setups under overcast, diffuse illumination conditions on August 30, 2021. All the images were stored in a camera-specific raw format. The cameras were fixed to a tripod approximately 1.3 m above the ground at each measurement point. The top of the image was oriented to the magnetic north using a compass. Each camera was pointed upwards and levelled using a two-axis bubble level, the focus setting on the lenses was set to infinity. The weather was dry, the ambient temperature was 15–20 °C, with almost no wind.

For camera setups I and II, the camera settings (shutter speed and ISO) were adjusted manually at each sampling point to take images with no overexposure and to keep pixel maximum value within the interquartile range of the camera's dynamic range (Lang *et al.*, 2017). This was necessary, because the incident radiation varied over time, with the sun rising and cloud cover thickness changing. Image blue-channel histogram was used to assess the necessity for adjustments. For camera setup III, an auto exposure bracketing function was used to take images. The base exposure was set to -2 EV at ±1 EV stop, resulting in a series of images at three consecutive EVs: -3, -2, and -1. However, later we discovered that this still caused overexposure on all of the photos at some measurement points because the camera was operated in a semiautomatic aperture priority mode.

Table 1. Camera setup specifications.

Tabel 1. Mõõtmisteks kasutatud kaamerad.

Variable	Camera setup		
	I	II	III
Camera model	Canon EOS 5D	Canon EOS 600D	Canon EOS 2000D
Fisheye Lens	Sigma 8 mm F3.5 EX DG	Sigma 4.5 mm F2.8 EX	Sigma 4.5 mm F2.8 EX
Camera height	1.3 m	1.3 m	1.3 m
Camera orientation	magnetic north	magnetic north	magnetic north
Initial ISO	640	400	100
Initial exposure compensation	0	0	-1
Initial shutter speed	1/32	1/60	Aperture priority
Image aquisition	single	single	auto-bracketing
F-stop	f/8	f/8	f/8
Light metering	Spot	Evaluative	Evaluative
Sensor size, pixels	12.8×10^6	18.0×10^6	24.1×10^6
Raw image radius*	1386	1450	1730

*Image radius on senor (pixels for 90 deg. zenith angle).

All acquired DHP images were processed with the free image processing software Hemispherical Project Manager (https://kosmos.ut.ee/en/services/free-hemispherical-software). The HSP implements the LinearRatio method (Cescatti, 2007) that takes into account the linear response to light on the camera sensors and implements the method for a single below-the-canopy-operated camera (LinearRatio$_{SC}$). As some acquired DHP for setup III encountered overexposure, we processed the images taken at -2 EV exposure compensation to reduce such effects. The pixel values were extracted with dcraw version 9.17 for setup I and version 9.28 (Coffin, 2018) for setups II and III, without colour interpolation and brightness scaling (-D switch). Dark frame values were subtracted (-K switch), and the 16-bit linear output was selected (-4 switch). Authentic blue pixels were sampled according to the sensor filter pattern. Circular fisheye images with linear projection were obtained after correcting for projection distortion and vignetting in setup I. No vignetting correction was applied for setups II and III because it had not been measured for them. However, all camera setups used the F-stop value of f/8, and in that configuration the vignetting effects are noticeable only at extreme viewing angles. Also, because of its principle, the LinearRatio$_{SC}$ method is much less sensitive to vignetting compared to methods based on threshold or pixel classification. For the LinearRatio$_{SC}$ unobscured sky pixel values were sampled from canopy gaps. The above-canopy reference images were then predicted using standard overcast sky models (ISO/CIE, 2004) fitted to sky radiance samples in combination with interpolation of pixel values similar to Lang *et al.* (2017, 2010). The canopy gap fraction P_o for each pixel was then calculated as

$$P_o = \frac{I_b}{I_a} \quad (1)$$

where I_a is the predicted above-canopy radiance and I_b is the measured below-canopy radiance.

Effective Plant Area Index calculation

The gap fraction function $P_o(\theta)$ can be used to calculate the effective LAI (L_e) using the formula proposed by Miller (1967):

$$L_e = 2\int_0^{\pi/2} -[lnP_o(\theta)]cos\theta sin\theta d\theta. \quad (2)$$

In our case we have gap fraction data over the hemisphere, sampled from 20 rings on the projected hemispherical image, each covering 4.5 degrees (0.0785 radians) of the zenith view angle. Therefore, we replace the integral calculation with a sum. Also, as we do not distinguish between foliage and woody material, we use the term effective Plant Area Index (PAI_e) instead of LAI:

$$PAI_e \approx -2\Delta\theta \sum_{n=1}^{N} lnP_o(\theta_n)cos\theta_n sin\theta_n, \quad (3)$$

where $\Delta\theta$ is constant 0.0785 radians in our case and θ_n is the view zenith angle for the n-th ring. We use Equation (2) to calculate the mean PAI_e for a set of images by taking the logarithm of the average of the gap fractions $\overline{P_o(\theta_n)}$ sampled from the images for each ring.

Results

The layout of image locations, i.e. sampling grid has some effect on the gap fraction estimate at stand level (Figure 2). The most significant differences between the sampling schemes occur near the zenith and smaller viewing angles. The differences in camera setups can also be noticed. Results from all setups correlate well with each other with R^2 values around 0.99, but setups I and II give a more similar gap fraction across view angles (average difference 0.005), whereas setup III deviates more from setups I and II (average difference 0.01 from setup I). Gap fractions from setups I and II consistently differ a little. Setup I almost always has a slightly smaller value for the gap fraction in all viewing zenith angles except the very small and the very large ones (Figure 2).

Based on the gap fraction, PAI_e estimates also vary between schemes and camera setups. The overall PAI_e, for the test site based on all schemes and all camera setups, comprising a total of 324 images, was 3.09 with a standard error (SE) of 0.02. Following Majasalmi *et al.* (2012), it is assumed that this very large set of 324 measurements is representative of the population mean. Here it is assumed that there is no influence of different measurement devices and operators on observations, however, later we show that each measurement series with a particular device had its own uncertainty characteristics. The ICOS and TERN schemes result in slightly smaller estimations for the PAI_e (2.99 and 3.03, respectively) than the NEON (3.26) scheme (Table 2). As the gap fraction estimation was consistently different between setups I and II, the resulting PAI_e estimation also reflects this difference, and the PAI_e values are consistently a little bit greater for setup I than for setup II. The PAI_e estimation for setup III stays close to the estimates of other two setups. Overall average PAI_e estimations for all setups and schemes ranged from 2.90 to 3.38, with standard errors ranging from 0.04 to 0.06 (Table 2).

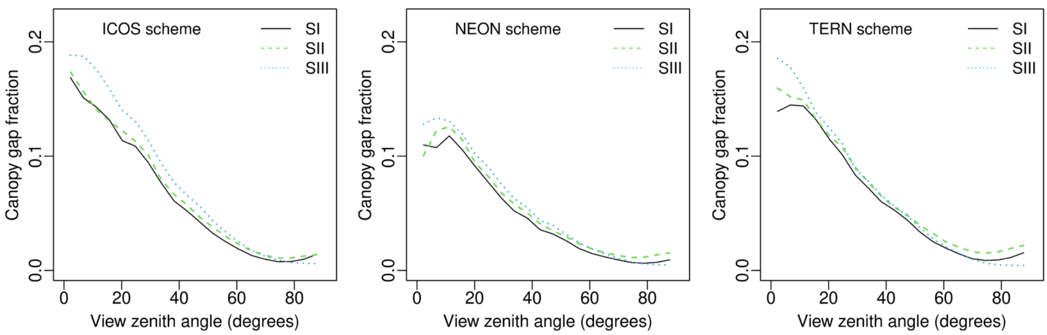

Figure 2. Comparison of the average gap fraction of the test stand with different camera setups (SI, SII, SIII) using ICOS, NEON and TERN sampling schemes.

Joonis 2. ICOS, NEON ja TERN võrgustikel kolme erineva kaameraga (SI, SII, SIII) *tehtud mõõtmistest arvutatud keskmised võrastiku läbipaistvused sõltuvalt vaatesuuna seniitnurgast.*

Table 2. Estimations of effective plant area index PAI_e for each sampling scheme taken with each setup and their corresponding standard errors (SE).

Tabel 2. Mõõtmisvõrgustike (ICOS, NEON, TERN) ja kaamerate (Setup I, II *ja* III) *kaupa võrastiku läbipaistvusest arvutatud efektiivne taimkatteindeks PAI_e ja selle standardviga (SE).*

Camera	Sampling network					
	ICOS		NEON		TERN	
	PAI_e	SE	PAI_e	SE	PAI_e	SE
Setup I	3.11	0.06	3.38	0.05	3.11	0.06
Setup II	2.99	0.06	3.22	0.05	2.94	0.05
Setup III	2.90	0.05	3.21	0.04	3.08	0.06

All three cameras took images at the same marked locations within a few minutes. Still, there are always slight deviations in positioning the cameras precisely at the same spot with identical levelling and orientation. This causes some variability in the recording of the scene content. Each camera operator processed the images taken with a particular camera. This also introduces some small variability into the results because (1) the markers of open sky pixel sampling markers can be freely chosen and (2) identification of canopy gaps at larger view zenith angles for extracting sky pixel samples requires some practicing and experience. However, Lang *et al.* (2013) show that the influence of randomness in open sky sampling point locations due to different analysts is marginal for the $LinearRatio_{SC}$. The PAI_e calculated from camera setups I and II has a very strong correlation (R^2 = 0.94) within image pairs, but setup III varied more in the results, giving often quite large deviations in the sampling points compared to setups I and II (Figure 3). Although setups I and II correlate well, the linear model fitted on the data has a slope around 0.91 and is also slightly shifted away from the 1 to 1 line, indicating a small systematic difference in the PAI_e.

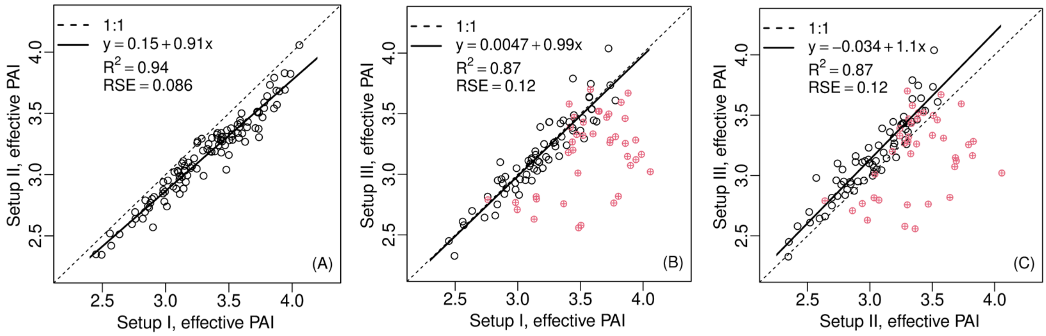

Figure 3. Effective plant area index PAI_e calculated from the data of three camera setups. RSE is the linear regression residual error. Overexposed measurements with Setup III are marked with red crossed circles and excluded from the regression.

Joonis 3. Mõõtmispunktides saadud efektiivse taimkatteindeksi PAI_e *võrdlus erinevate kaamerate* (Setup I, II *ja* III) *kaupa. Kaamera III ülevalgustatud mõõtmised on tähistatud punaste ringristidega ja regressioonimudelist välja jäetud. RSE on mudeli jääkviga.*

As the forest stand is natural, i.e. not perfectly homogeneous, it can be expected that the PAI_e obtained at different measurement points would vary, for example for setup I, the PAI_e calculated from single images ranges from 2.45 to 4.06 (Figures 4, 5, 6). However, the PAI_e includes both – the true value and uncertainty that is introduced during the measurements and data processing.

Setup III had a problem with overexposure due to the semiautomatic imaging mode. Some images were out of focus – possibly due to accidental turning of the focus wheel, resulting in loss of detail in smaller gaps, leaves and branches (Figure 8). Even though setup III had the highest pixel resolution, the loss of small details due to the wrong focus setting combined with overexposure did contribute to inconsistent results at many sampling points demonstrated by PAI_e values compared to setups I and II (Figure 3B, C). We identified overexposed measurements of setup III based on possible maximum pixel values according to the camera radiometric resolution (also known as bit depth) and found that the concordance of the rest (i.e. correct measurements with setup III) with the other measurements was strong (Figure 3B, C).

The impact of image overexposure on the measurements of the canopy gap fraction and consequently PAI_e was not constant. The PAI_e of some of the overexposed measurements was not much different from setup I and setup II, which can be attributed to the magnitude of overexposure and also to the amount of mixed pixels in the scene where "burn-in" effects occur first. Additionally, the out-out-of-focus problem tended to fill small canopy gaps of few pixels in size, effectively decreasing the canopy gap fraction. Therefore, it is the responsibility of the camera operator to keep the camera in the linear sensitive range of the sensor to avoid overexposure and systematic errors in the canopy gap fraction and PAI_e.

Table 3. Linear relationships between effective plant area index between three camera setups by sampling schemes and using only correct (C) i.e. non-overexposed images of setup III or all (A). RSE is model residual error and N is the number of observations.

Tabel 3. Lineaarsed regressioonmudelid kaamerate ning mõõtmisskeemide kaupa. Kaamera III mudelid on antud kõikide (A) või ainult korrektsete mõõtmiste ehk ülevalgustamata piltide andmete (C) järgi. RSE on mudeli jääkviga ning N on vaatluste arv.

Camera setup		Sampling		Linear regression $S_y=a+bS_x$				
S_x	S_y	Network	Subset	R^2	a	b	RSE	N
I	II	ICOS	A	0.97	0.21	0.89	0.06	36
I	II	NEON	A	0.90	0.05	0.94	0.10	36
I	II	TERN	A	0.92	0.21	0.88	0.09	36
I	III	ICOS	A	0.28	1.55	0.45	0.27	36
I	III	ICOS	C	0.92	0.10	0.96	0.10	21
I	III	NEON	A	0.23	1.90	0.40	0.23	36
I	III	NEON	C	0.84	-0.52	1.15	0.12	23
I	III	TERN	A	0.71	0.55	0.81	0.18	36
I	III	TERN	C	0.84	0.10	0.97	0.13	24
II	III	ICOS	A	0.29	1.44	0.50	0.27	36
II	III	ICOS	C	0.93	0.02	1.02	0.09	21
II	III	NEON	A	0.17	2.15	0.35	0.24	36
II	III	NEON	C	0.85	-0.73	1.28	0.12	23
II	III	TERN	A	0.77	0.36	0.92	0.16	36
II	III	TERN	C	0.87	0.16	1.01	0.12	24

The PAI_e values obtained at each sampling point correlated well between setups I and II with R^2 values of 0.97 for ICOS, 0.89 for NEON, and 0.92 for TERN (Table 3). The differences in correlation are probably due to the uncertainty of measurements and cannot be attributed to a particular sampling scheme. Overexposed measurements decreased substantially the correlation of setup III with the others. However, in the subset of correct measurements that did not suffer from overexposure, the correlations were of the same strength than between setup I and setup II (Table 3).

As we noticed some systematic differences in camera setups I and II, we conducted an experiment where the images of the ICOS scheme were cross-processed by the camera operators to see if there was some human error or bias. We found a small difference in the estimated gap fraction around the large viewing angles (Figure 8) but overall, the results are not statistically different from each other with a one-tail t-test p-value of 0.486.

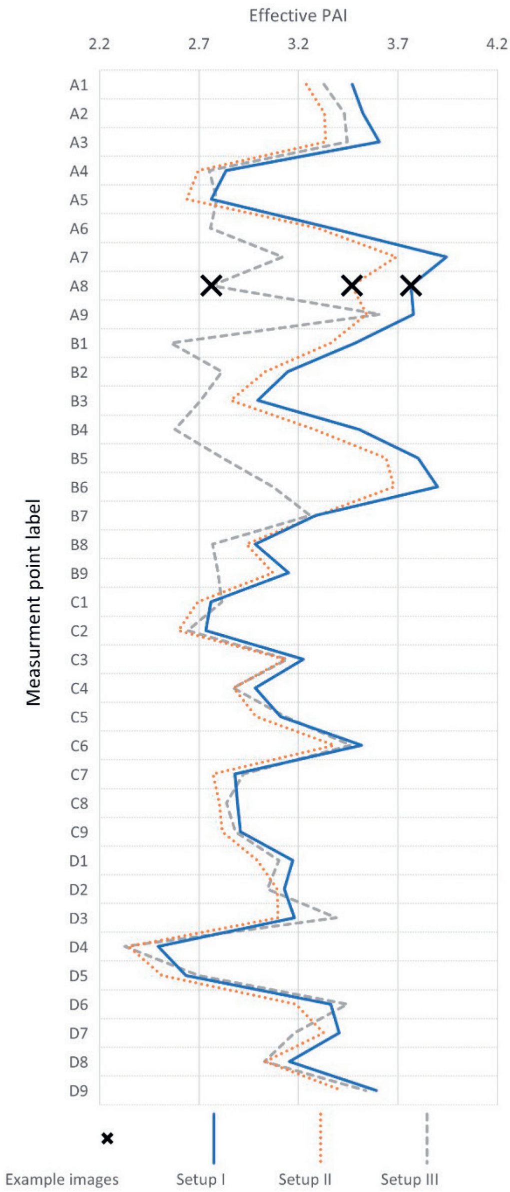

Figure 4. PAI_e values from three camera measurements for the ICOS scheme and the locations of the sample images shown in Figure 7.

Joonis 4. Efektiivse taimkatteindeksi PAI_e väärtused mõõtmiste jadas ICOS võrgustiku punktides. Ristiga on näidatud joonisel (8) toodud näidispildi mõõtmispunkt.

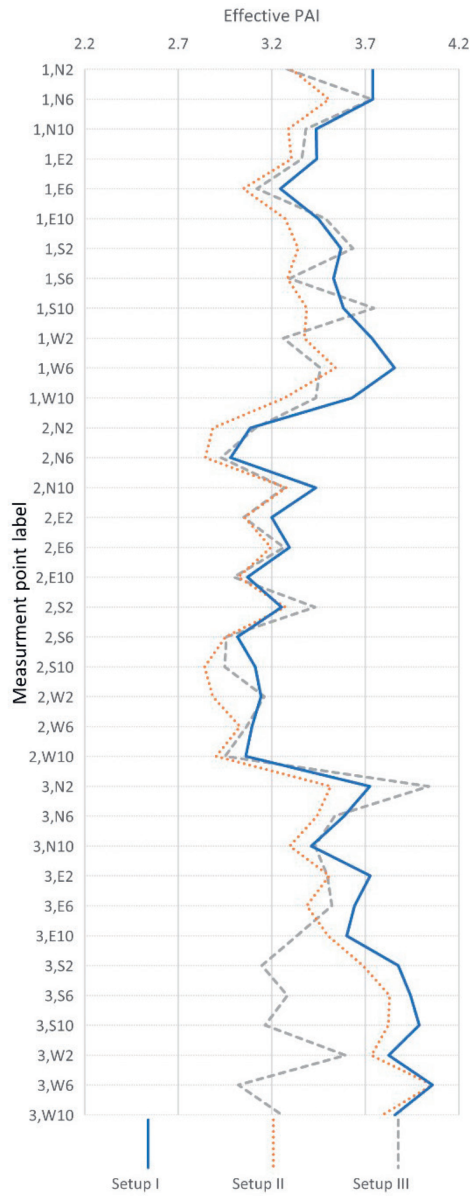

Figure 5. PAI_e values from three camera measurements for the NEON scheme.

Joonis 5. Efektiivse taimkatteindeksi PAI_e väärtused mõõtmiste jadas NEON võrgustiku punktides.

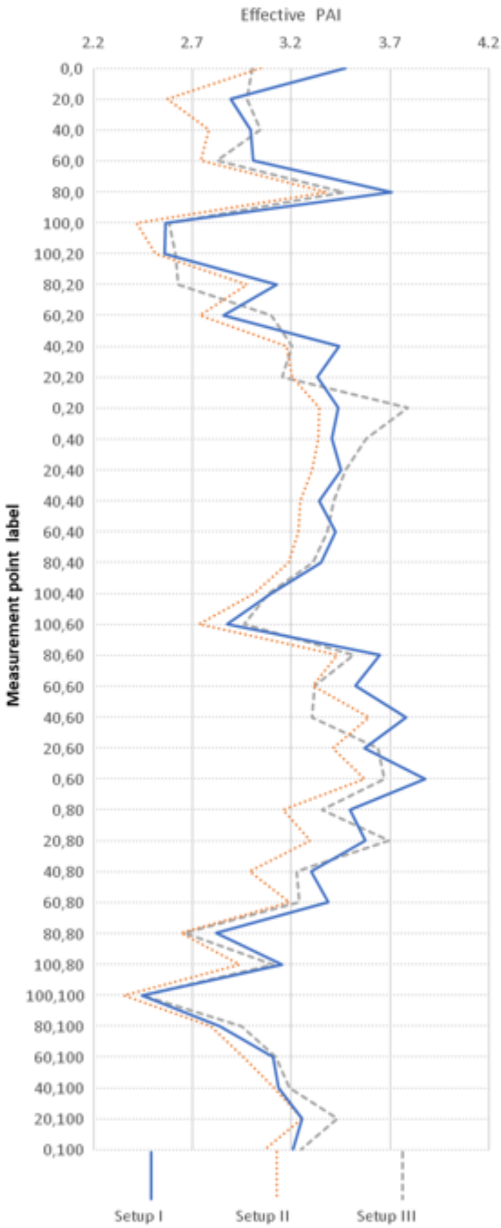

Figure 6. PAI_e values from three camera measurements for the TERN scheme.

Joonis 6. Efektiivse taimkatteindeksi PAI_e väärtused mõõtmiste jadas TERN võrgustiku punktides.

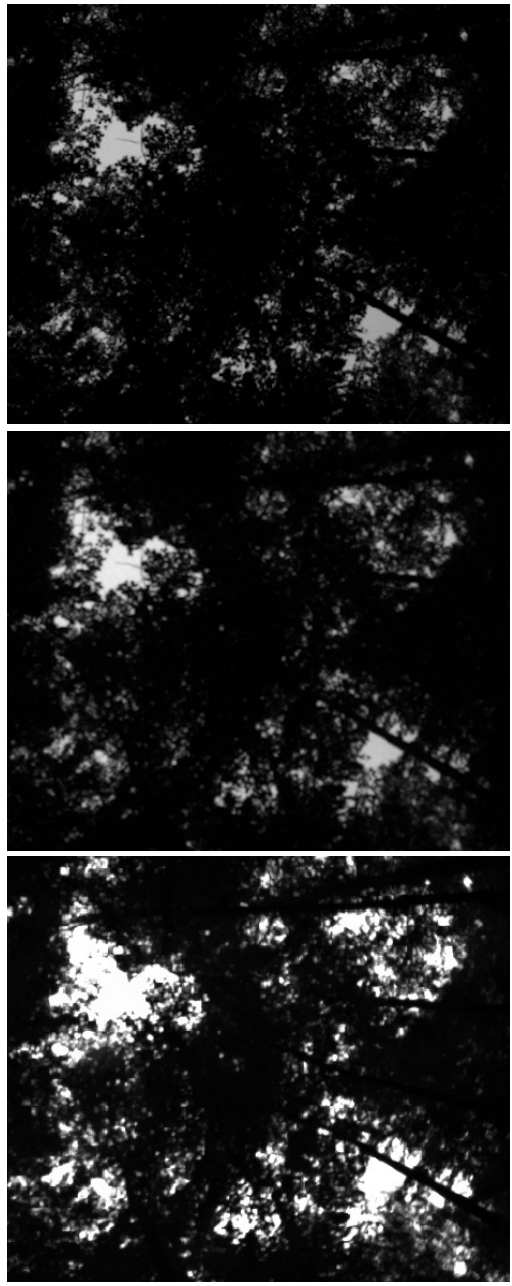

Figure 7. Zoomed-in central parts of the blue channel of the photos taken from ICOS point A8 with setup I (A), setup II (B), and setup III (C).

Joonis 7. Suurendus kaameratega (I, II ja III) ICOS võrgustiku punktis A8 tehtud ülesvõtte keskosast. Kaamera III pildil on näha tugeva ülevalgustatuse ilminguid.

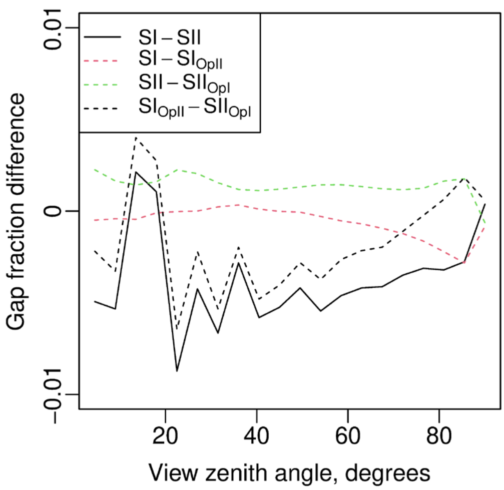

Figure 8. Comparison of differences in average gap fractions in the ICOS scheme calculated from measurements with setup I and setup II and processed by the camera operators OpI or OpII. The influence of the image analyst is small compared to the camera factor.

Joonis 8. ICOS mõõtmisvõrgu andmetel saadud võrastiku keskmise läbipaistvuse erinevus kaamerate I ja II andmetel. Sama kaamera piltide töötlemisel on operaatori mõju (OpI, OpII) väike võrreldes kaamera faktoriga.

Discussion and Conclusion

An estimation of plant or leaf area index for a test site using optical measurements of canopy gap fraction or gap size distribution is influenced by many factors that introduce uncertainty into the results. In our study, we focused on the sampling design, field measurements, and image processing. Sampling design, in an ideal case, (1) provides that enough measurements are made to obtain sufficiently narrow confidence intervals for the estimates and (2) ensures that repeated measurements in time series are comparable by fixing, for example, the arrangement of permanent and random sampling points. The stage of field measurements involves uncertainties related to configuring cameras, locating measurement points, setting up the camera on the point, observing illumination conditions according to the measurement protocol, determining exposure settings to keep the camera in its linear sensitivity range, and the physical process of taking images. Image processing involves extracting the data from camera output files, applying radiometric and geometric corrections, selecting the image processing method and its parameters and software, and calculating the gap fraction according to the view zenith angle from the processed images for the Equation (2). Prediction of the true green leaf area index further from the canopy gap fraction includes another wide range of models and methods.

We used three different sampling schemes and obtained the PAI_e in the range of 2.99–3.26 for the Järvselja RAMI birch stand. The result is close to Kuusk *et al.* (2009), who reported PAI_e 2.94 measured at nine positions with the LAI-2000 instrument within the same test site. The small increase in PAI_e values compared to Kuusk *et al.* (2009) can be explained by a growth of dominant and lower tree layers during the period (>15 years) between the measurements (Lang & Pisek, 2019). The PAI_e derived from ICOS and TERN sampling schemes were more similar to each other (two-tailed t-test p-value 0.229) than NEON (t-test p-value < 0.00001) results (Table 2). The difference between NEON results compared to the other schemes may be explained by the distribution of the sampling points in the forest. The NEON scheme has three tightly packed locations in the forest where images are taken, whereas TERN and ICOS are more spread out over the whole plot (Figure 1). With NEON, the initial selection of the three sub-section locations is important because if two or all three locations fall into either more open or closed canopy areas, the sample is not representative of the forest as a whole. Even though we followed the scheme layout instructions carefully, with our testing, two of the locations happened to have rather closed canopy conditions and the resulting images gave on average a smaller gap fraction when compared to the ICOS and TERN sampling schemes (Figure 2). The NEON protocol uses this kind of sampling in conjunction with a second larger set of distributed plots that are sampled less frequently but cover more of the forests. The tower plots described in the NEON protocol can give a good time series of the area near the sampling points, but they should be viewed together with the distributed plots results to properly represent a forest site.

Proper camera configuration is essential to get consistent and comparable measurements. As our goal was to measure incident radiation as precisely as possible, it was necessary to avoid over- or underexposing the image. In our testing, setup III illustrated possible issues with overexposed and out-of-focus images where smaller details of the canopy were often lost (Figure 7C). This resulted in occasional inconsistent results when compared to setups I and II, which had a very good correlation with each other (Figure 3A). When tested afterwards, reducing the focus setting of the camera decreased the effective PAI_e by 1.3% on average when the focus was turned down from infinity to 0.2 meters. When intentionally overexposing the images the PAI_e decreased significantly. When an image with no overexposed pixels was compared to another one that had 0.1% of pixels overexposed to the maximum digital value of the sensor, the PAI_e decreased by around 1.7%. When the amount of overexposed pixels was around 0.4%, the PAI_e decreased substantially by 14%. Here we see that for obtaining data for the canopy gap fraction it is crucial to operate hemispherical cameras in their linear sensitive range.

Our intercomparison test allowed us to search for possible influences of cameras and image analysts on the canopy gap fraction and calculated PAI_e. There was very strong correlation between the PAI_e of setups I and II with a small systematic difference. In a time series this could be interpreted as a possible change in the PAI_e, but in our experiment the measurements were done almost within a few minutes in time that excludes the change in the PAI_e. For image processing we used a well-established method $LinearRatio_{SC}$ that, by its principle, is an analogue for LAI-2000 when compared to various threshold-based and pixel classification-based algorithms. To apply $LinearRatio_{SC}$ the image analyst has to place sky pixel sampling marks for constructing open sky reference which involves a subjective decision to some extent.

We tested the influence of operator subjectivity by cross-reprocessing the ICOS scheme images that were taken with setup I and II by corresponding operators. However, no statistically relevant differences were found in the gap fraction calculated from the same set of images processed by two different people (Figure 8). This indicates that there is a more fundamental reason stemming from the raw images or cameras themselves. We also tested the effects of vignetting and projection models, subtracting the dark images, and the effects of different versions of dcraw. They all had negligible or no impact on the results. Setup I consistently had a little but smaller gap fraction than setup II. Addressing all these possible sources of uncertainty, we conclude that the difference may be caused by light scattering and colour crosstalk within cameras. Another possible reason could be a small systematic difference in camera height over the ground or vertical levelling during field measurements. For example, a two-degree error in camera levelling changes the path length at 57° view zenith angle up to three metres (10%) in the stand. As a conclusion, we recommend always to carry out intercomparison measurements with old and new cameras when devices are upgraded.

Overall, we illustrate that the three different employed schemes produce comparable results for estimating the gap fraction and PAI_e. Although different setups and schemes gave differing results, with Anova Two-Factor test p-values <0.001, there was no connection between the camera setup used and the scheme (p-value 0.178). Our testing shows that more evenly spread out sampling schemes are more consistent with each other, exemplified by ICOS and TERN, and could be more representative of the overall conditions of the forest. The results vary when different cameras with different operators are used, but it appears that 36 images employed by all three setups are enough to deliver an average with sufficiently narrow confidence limits. It depends on the application what type of cameras and how high accuracy of calibration is required. From this study we cannot conclude which scheme or camera setup is best used in the field, because all these established schemes vary slightly in their intended use and purpose and are not necessarily intended to yield site level mean estimates. But we did conclude that some layout schemes may have inherited problems when applied to estimate the PAI_e for our 1-hectare plot. The CEOS Land Product Validation Subgroup (Morisette *et al.*, 2006) suggests in their proposed framework, for validating LAI products, to use a two-staged sampling design. In the case of NEON and ICOS, the circular and cross shaped compact sampling areas would be considered elementary sampling units used together with high spatial resolution satellite data to capture the variability in the site extent. These two sampling schemes are not directly designed to capture the average PAI_e for a 1-hectare site as in our case.

The CEOS LPV is currently in the process of selecting supersites with a fully characterized land surface and vegetation cover for the parameterization of 3D radiative transfer models. Our study contributes towards establishing the procedures for uncertainty estimation by evaluating potential systematic errors stemming from collecting in situ measurements with DHP using different scheme designs, methods and devices currently in use at most LPV Supersites.

Future work can include efforts to investigate the impact of sampling schemes on the LAI estimation of forests from other indirect LAI measurement methods (e.g. terrestrial laser scanner and LAI-2200). Ground-Based Observations for Validation (GBOV) of Copernicus Global Land Products (GBOV, 2023) uses schemes studied in this paper to validate its decametric and hectometric satellite-derived LAI products (Brown *et al.*, 2020) and thus it is important to study these schemes. More comparisons between measurement methods and data processing methods would be useful in determining the most reliable ways to gather data on the gap fraction. Forest plots with different plant functional types may also be included to consolidate the findings of this study.

Acknowledgements. This study was supported by the Estonian Research Council grant PRG 1405. SZ received financial support from the Academy of Finland Flagship Programme (Forest-Human-Machine Interplay – Building Resilience, Redefining Value Networks and Enabling Meaningful Experiences (UNITE); grant number 337127). We thank reviewers for their valuable comments, which helped to improve the manuscript.

References

Brown, L.A., Meier, C., Morris, H., Pastor-Guzman, J., Bai, G., Lerebourg, C., Gobron, N., Lanconelli, C., Clerici, M., Dash, J. 2020. Evaluation of global leaf area index and fraction of absorbed photosynthetically active radiation products over North America using Copernicus Ground Based Observations for Validation data. – Remote Sensing of Environment, 247, 111935. https://doi.org/10.1016/j.rse.2020.111935.

Calders, K., Origo, N., Disney, M., Nightingale, J., Woodgate, W., Armston, J., Lewis, P. 2018. Variability and bias in active and passive ground-based measurements of effective plant, wood and leaf area index. – Agricultural and Forest Meteorology, 252, 231–240.

Cescatti, A. 2007. Indirect estimates of canopy gap fraction based on the linear conversion of hemispherical photographs: Methodology and comparison with standard thresholding techniques. – Agricultural and Forest Meteorology, 143, 1–12. https://doi.org/10.1016/j.agrformet.2006.04.009.

Chen, J.M. 1996. Optically-based methods for measuring seasonal variation of leaf area index in boreal conifer stands. – Agricultural and Forest Meteorology, 80(2–4), 135–163. https://doi.org/10.1016/0168-1923(95)02291-0.

Chen, J.M., Black, T.A. 1992. Defining leaf area index for non-flat leaves. – Plant, Cell & Environment, 15(4), 421–429. https://doi.org/10.1111/j.1365-3040.1992.tb00992.x.

Coffin, D. 2018. Decoding raw digital photos in Linux. [WWW document]. – URL https://www.dechifro.org/dcraw/. [Accessed 3 January 2023].

Fang, H., Baret, F., Plummer, S., Schaepman-Strub, G. 2019. An overview of global leaf area index (LAI): Methods, products, validation, and applications. – Reviews of Geophysics, 57(3), 739–799. https://doi.org/10.1029/2018RG000608.

Fernandes, R., Plummer, S., Nightingale, J., Baret, F., Camacho, F., Fang, H., Garrigues, S., Gobron, N., Lang, M., Lacaze, R., LeBlanc, S., Meroni, M., Martinez, B., Nilson, T., Pinty, B., Pisek, J., Sonnentag, O., Verger, A., Welles, J., Weiss, M., Widlowski, J.L. 2014. Global leaf area index product validation good practices. Version 2.0. – Schaepman-Strub, G., Román, M., Nickeson, J. (eds.). Good Practices for Satellite-Derived Land Product Validation. Geneva, Switzerland, Land Product Validation Subgroup (WGCV/CEOS). 76 pp. https://lpvs.gsfc.nasa.gov/PDF/CEOS_LAI_PROTOCOL_Aug2014_v2.0.1.pdf.

GBOV. 2023. Ground-based observations for validation (GBOV) of Copernicus global land products. [WWW document]. – URL https://land.copernicus.eu/global/gbov. [Accessed 8 January 2023].

GCOS-138. 2010. Implementation plan for the global observing system for climate in support of the UNFCCC (2010 Update). WMO/TD-No. 1523. Geneva, Switzerland, GCOS Secretariat, World Meteorological Organization (WMO). 180 pp.

Gielen, B., Op de Beeck, M., Michilsens, F., Papale, D. 2017. ICOS ecosystem instructions for ancillary vegetation measurements in forest (version 20200330). ICOS Ecosystem Thematic Centre. [WWW document]. – URL https://doi.org/10.18160/4ajs-z4r9. [Accessed 10 January 2023].

ISO/CIE. 2004. ISO5469:2004(E)/CIE S 011/E:2003. Spatial distribution of daylight – CIE standard general sky. Geneva, Switzerland / Vienna, Austria, ISO and CIE. 7 pp.

Karan, M. 2015. Supersites vegetation monitoring protocols. TERN Australian SuperSite Network. Version 1.21. [WWW document]. – URL https://www.tern.org.au/wp-content/uploads/SuperSites_Vegetation_Monitoring_Protocols_Ver1.21.pdf. [Accessed 8 January 2023].

Kuusk, A., Kuusk, J., Lang, M. 2009. A dataset for the validation of reflectance models. – Remote Sensing of Environment, 113(5), 889–892. https://doi.org/10.1016/j.rse.2009.01.005.

Kuusk, A., Lang, M., Kuusk, J. 2013. Database of optical and structural data for the validation of forest radiative transfer models. – Light Scattering Reviews, 7, 109–148.

Lang, M., Kodar, A., Arumäe, T. 2013. Restoration of above canopy reference hemispherical image from below canopy measurements for plant area index estimation in forests. – Forestry Studies / Metsanduslikud Uurimused, 59, 13–27.

Lang, M., Kuusk, A., Kaha, M., Pisek, J., George, J.-P., Kiviste, A., Laarmann, D., Türk, K., Arumäe, T. 2021. Changes during twelve years in three mature hemiboreal stands growing in a radiation model intercomparison test site, Järvselja, Estonia. – Forestry Studies / Metsanduslikud Uurimused, 74, 112–122.

Lang, M., Kuusk, A., Mõttus, M., Rautiainen, M., Nilson, T. 2010. Canopy gap fraction estimation from digital hemispherical images using sky radiance models and a linear conversion method. – Agricultural and Forest Meteorology, 150(1), 20–29. https://doi.org/10.1016/j.agrformet.2009.08.001.

Lang, M., Nilson, T., Kuusk, A., Pisek, J., Korhonen, L., Uri, V. 2017. Digital photography for tracking the phenology of an evergreen conifer stand. – Agricultural and Forest Meteorology, 246, 15–21.

Lang, M., Pisek, J. 2019. Tracking the long-term structure changes of a mature deciduous broadleaf forest stand using digital hemispherical photography. – Forestry Studies / Metsanduslikud Uurimused, 70, 80–87.

Liu, J., Li, L., Akerblom, M., Wang, T., Skidmore, A., Zhu, X., Heurich, M. 2021. Comparative evaluation of algorithms for leaf area index estimation from digital hemispherical photography through virtual forests. – Remote Sensing, 13(16), 3325. https://doi.org/10.3390/rs13163325.

Majasalmi, T., Rautiainen, M., Stenberg, P., Rita, H. 2012. Optimizing the sampling scheme for LAI-2000 measurements in a boreal forest. – Agricultural and Forest Meteorology, 154–155, 38–43. https://doi.org/10.1016/j.agrformet.2011.10.002.

Meier, C., Jones, K. 2018. TOS protocol and procedure: Measurement of leaf area index. [WWW document]. – URL https://data.neonscience.org/documents/10179/1883155/NEON.DOC.014039vM/94cd2218-598c-935f-829e-5003d7b25950. [Accessed 8 January 2023].

Miller, J.B. 1967. A formula for average foliage density. – Australian Journal of Botany, 15(1), 141–144.

Morisette, J.T., Baret, F., Privette, J.L., Myneni, R.B., Nickeson, J.E., Garrigues, S., Shabanov, N.V., Weiss, M., Fernandes, R.A., Leblanc, S.G., Kalacska, M., Sanchez-Azofeifa, G.A., Chubey, M., Rivard, B., Stenberg, P., Rautiainen, M., Voipio, P., Manninen, T., Pilant, A.N., Lewis, T.E., Iiames, J.S., Colombo, R., Meroni, M., Busetto, L., Cohen, W.B., Turner, D.P., Warner, E.D., Petersen, G.W., Seufert, G., Cook, R. 2006. Validation of global moderate-resolution LAI products: a framework proposed within the CEOS land product validation subgroup. – IEEE Transactions on Geoscience and Remote Sensing, 44(7), 1804–1817. https://doi.org/10.1109/TGRS.2006.872529.

Nackaerts, K., Coppin, P., Muys, B., Hermy, M. 2000. Sampling methodology for LAI measurements with LAI-2000 in small forest stands. – Agricultural and Forest Meteorology, 101(4), 247–250.

Widlowski, J.-L., Mio, C., Disney, M., Adams, J., Andredakis, I., Atzberger, C., Brennan, J., Busetto, L., Chelle, M., Ceccherini, G., Colombo, R., Côté, J.-F., Eenmäe, A., Essery, R., Gastellu-Etchegorry, J.-P., Gobron, N., Grau, E., Haverd, V., Homolová, L., Huang, H., Hunt, L., Kobayashi, H., Koetz, B., Kuusk, A., Kuusk, J., Lang, M., Lewis, P.E., Lovell, J.L., Malenovský, Z., Meroni, M., Morsdorf, F., Mõttus, M., Ni-Meister, W., Pinty, B., Rautiainen, M., Schlerf, M., Somers, B., Stuckens, J., Verstraete, M.M., Yang, W., Zhao, F., Zenone, T. 2015. The fourth phase of the radiative transfer model intercomparison (RAMI) exercise: Actual canopy scenarios and conformity testing. – Remote Sensing of Environment, 169, 418–437.

Zou, J., Hou, W., Chen, L., Wang, Q., Zhong, P., Zuo, Y., Luo, S., Leng, P. 2020. Evaluating the impact of sampling schemes on leaf area index measurements from digital hemispherical photography in *Larix principis-rupprechtii* forest plots. – Forest Ecosystems, 7, 52. https://doi.org/10.1186/s40663-020-00262-z.

Digitaalsete poolsfäärikaamerate seadistuse ning ICOS, NEON ja TERN skeemi mõõtmispunktide paigutuse mõju tiheda lehtpuumetsa taimkatteindeksi hindamisele

Mihkel Kaha, Mait Lang, Shaohui Zhang ja Jan Pisek

Kokkuvõte

Taimestiku lehepinnaindeks (LAI) on kasutuses paljudes fotosünteesi - ja evapotranspiratsiooni mudelites. LAI hindamiseks suurtel aladel kasutatakse kaugseireandmetele tuginevaid meetodeid, mille sisendi ja ka tulemuse valideerimiseks on vaja maapeal tehtud täpseid mõõtmisi. Selleks kasutatakse tavaliselt mittedestruktiivseid optilisi meetodeid, nagu poolsfäärikaamerate abil võrastiku läbipaistvuse (P_o) nurkolenevuse mõõtmine, millest saadakse esmalt efektiivne taimkatteindeks PAI_e. Siinses uurimuses testiti mõõtmiskohtade paigutuse ning kaamera seadistuse mõju võrastiku läbipaistvuse ja PAI_e mõõtmistulemustele Järvseljal asuvas tihedas lehtpuumetsas (Kuusk *et al.*, 2009, 2013; Lang & Pisek, 2019; Lang *et al.*, 2021).

Mõõtmispunktid paigutati Integrated Carbon Observation System (ICOS) (Gielen *et al.*, 2017), National Ecological Observatory Network (NEON) (Meier & Jones, 2018) ja Terrestrial Ecosystem Research Network (TERN) (Karan, 2015) skeemide järgi (joonis 1). Võrastikust läbituleva valguse mõõtmised tehti hajusa valgustatusega pilves ilmaga 30. augustil 2021 kolme erineva kaameraga (tabel 1). LinearRatio meetodi abil saadi piltidelt andmed võrastiku läbipaistvuse (1) ja PAI_e (2, 3) arvutamiseks.

Mõõtmispunktide komplekti kaupa saadi erinevate kaameratega P_o ja PAI_e üsna lähedased väärtused (joonis 2, tabel 2), kuigi NEON võrgustiku kolm kompaktselt paigutuvat mõõtmispunktide kobarat olid sattunud keskmisest tihedamasse puistu ossa ning kaamera SIII andmetes esines poolautomaatse särituse kasutamise tõttu ülevalgustamist (joonis 3, joonis 7). Korrektselt tehtud mõõtmiste puhul saadi erinevate kaameratega sarnane PAI_e (tabel 3). Testala puistu võrastiku tihedus varieerus mõõtmispunktide vahel ning see kajastus ka kõikide kaamerate poolsfääripiltidel (joonised 4–6). Kaamerate SI ja SII tulemustes oli püsivalt mõningane süstemaatiline erinevus, mille põhjusena kahtlustati algselt piltide töötlejate subjektiivseid otsuseid LinearRatio meetodi rakendamisel, kuid see ei leidnud ristvõrdluse katses kinnitust (joonis 8). Erinevuse põhjusteks tuleb pigem pidada pisikesi süstemaatilisi vigu kaamerate paigutamises ja loodimises metsas ning kaameras ja optikasüsteemis hajuva valguse mõju. Tööst saab teha kolm põhilist järeldust. Mõõtmispunktide paigutus ja arv tuleb valida sõltuvalt sellest, kas on vaja iseloomustada võimalikult täpselt konkreetset punkti või puistut tervikuna. Fotografeerimisel peab kaamera operaator jälgima, et kaamera töötaks mõõtmistel selle lineaarse tundlikkuse vahemikus, mis tagab moonutamata andmed võrastiku läbipaistvuse kohta. Kaamerate uuendamisel mõõtmisprojektides on äärmiselt oluline teha kaameratega korraga koos võrdlusmõõtmisi, et tuvastada mõõtmisseadme mõju tulemustele.